Electron-positron correlations in silicon

A. Rubaszek*
W. Trzebiatowski Institute of Low Temperature and Structure Research, Polish Academy of Sciences, P.O. Box 1410, 50-950 Wrocław 2, Poland

Z. Szotek† and W. M. Temmerman‡
Daresbury Laboratory, Daresbury, Warrington, WA4 4AD, Cheshire, United Kingdom
(Received 3 November 1999; revised manuscript received 3 January 2000)

A number of approaches to treat the electron-positron correlation effects is used to study electron-positron momentum densities and positron annihilation rates in bulk silicon. Also, the nonlocal effects are explicitly taken into account within the weighted density approximation (WDA), giving rise to nonlocal state-selective electron-positron correlation functions. The WDA results for the electron-positron momentum densities and annihilation rates are compared to the experimental data and to calculations performed within the independent-particle model and local-density approximation. Additionally, the generalized-gradient approximation is used to calculate nonlocal, but state independent, quantities. The importance of nonlocality and state-dependence of the electron-positron correlation functions, and the role of the positron wave function, are discussed in detail.

I. INTRODUCTION

The positron lifetime τ, and angular correlation of positron annihilation radiation (ACAR) techniques, have become very useful tools for studying electronic structure of metals.[1] Due to their technological importance, many elemental and compound semiconductors have also been fairly extensively studied using positron annihilation spectroscopies (see Refs. 2–16, and references cited therein). However, as in the case of metals, the interpretation of positron annihilation data for semiconductors is not easy, and to extract information on the electron momentum density (EMD) and electron charge density of the studied systems, both the electron-positron (e-p) interaction and positron wave function[5] have to be considered explicitly. The importance of these effects becomes especially apparent when comparing ACAR spectra with Compton profiles (CP's).[7,10,16] In this paper we present a detailed study of the influence of these effects on the electron momentum density, charge distribution, and other positron annihilation characteristics in bulk silicon.

For semiconductors the importance of the positron wave function for positron annihilation characteristics follows almost naturally from crystal structure. The group-IV elemental semiconductors (Si, Ge) and the group-III-V compound semiconductors (e.g., GaAs) crystallize in open diamond or zinc-blende structures. Therefore, unlike electrons, a positron in these systems is most likely to be found in the interstitial region. In fact, over 70% of the positron distribution is located in this region.[17] In semiconductors the effect of the positron wave function is often associated with the characteristic dips observed in the low-momentum region of the ACAR spectra. Specifically, all one- (1D), two- (2D), and three-dimensional (3D) (reconstructed) ACAR spectra, measured for elemental and compound semiconductors, show, in the low-momentum region, dips and valleys along the [110] and [100] directions, while along the [111] direction a sharp peak is observed. The size of these dips, which varies among different semiconductors, has been analyzed using group-theoretical considerations.[6] The fact that these dips are somewhat shallower in the group-III–V semiconductors than in Si and Ge has been attributed to symmetry lowering, from O_h^7 in the group-IV semiconductors to T_d^2 in the III-V compound semiconductors. However, Panda and co-workers,[7,10] comparing the CP data for Si, Ge, and GaAs, arrived at the conclusion that the slopes of the dips in the ACAR spectra cannot be explained in terms of the band contributions alone, but are most probably due to the positron density distribution. Also, the e-p correlations are expected to contribute substantially to the different shapes of the ACAR spectra in these systems, in the low-momentum region.

Although electron-positron correlations lead to a significant change in the electron momentum density, it is the independent-particle model (IPM) that has been most commonly used in calculations of the electron-positron momentum density in semiconductors.[2,3,6,7] This approach takes into account the effect of the positron wave function, but neglects completely the e-p correlations, thus giving rise to considerable differences between theory and experiment, especially in the low-momentum region and at the Jones zone faces.[3,4,6,7] As to the differences of the ACAR spectra in the low-momentum region, Fujiwara was the first to point out deenhancement effects in the high-momentum region of the ACAR spectra in silicon.[4] However, only in more recent calculations of momentum densities in semiconductors have two-particle correlation functions, taking account of the $e-p$ correlations, been considered either within the local-density approximation (LDA)[8,11,12] or, including some form of nonlocality, within the generalized-gradient approximation (GGA),[10,11] as described in Refs. 13 and 14. Nevertheless, these correlations have only been included in a state-independent form. By state independence one means that e-p correlation functions, as employed in calculations of Refs. 8, 10, and 11, have been independent of the initial electron Bloch state. In the application to Si, these state-independent correlation functions gave rise in the low-momentum region to almost constant enhancement factors,[10] defined as a ratio of the e-p momentum density, $\rho(\mathbf{p})$, to its IPM counterpart. Note that these constant enhancement factors have also been

 ©2000 The American Physical Society

obtained in the GGA approach, where the *e-p* correlations have been treated nonlocally. In the present paper, however, we shall argue that it is the state dependence of the correlation functions that is of paramount importance for obtaining the correct low-momentum behavior of the ACAR spectra in Si. The arguments follow from the fact that the valence electrons in Si are mostly *sp* like, giving rise to nearly parabolic valence bands.[2] It has been shown by general theoretical considerations,[18] and confirmed by experiments for simple metals,[19] that for nearly free electrons the state dependence of *e-p* correlation functions has an important influence on the shape of the valence contribution to $\rho(\mathbf{p})$ in the low-momentum region. Here it will be shown that the state dependence of the *e-p* correlation functions, whether local or nonlocal, is the most important factor for obtaining a correct description of the experimentally observed ACAR spectra in semiconductors. The nonlocal effects are important for core electron but also reflect the localization of the valence electron density along the tetrahedral bonds. Nevertheless, in silicon the core electron contribution to the annihilation characteristics is very small (below 3%), and therefore nonlocal effects are not expected to have an important influence on $\rho(\mathbf{p})$, but can be seen in the core part of the total annihilation rate, $\lambda = 1/\tau$.[17]

In the present paper we implement the weighted-density approximation (WDA)[17] to calculate the nonlocal state-dependent *e-p* correlation functions, and with them the *e-p* momentum density $\rho(\mathbf{p})$ and positron lifetime τ for bulk Si. We discuss in detail the effect of nonlocality of the *e-p* correlations on the resulting positron annihilation characteristics. Additionally, following the approach of Daniuk *et al.*,[20] we calculate the latter quantities within the local density approximation using the state-selective enhancement factors (SEF's), while calculating the *e-p* correlation functions. Note that since the state selectivity of the correlation functions is usually expressed through the dependence on the electron energy eigenvalues, the state-selective correlation functions are in fact the selective energy functions.[21] These results are further compared to the calculations performed within IPM, and the LDA and GGA approaches, where the *e-p* correlation functions are state independent, namely, they have been calculated with the constant enhancement factors (CEF), with respect to their dependence on the electron state $\mathbf{k}j$. Thus, in contrast to the state-selective *e-p* correlation functions, the state-independent *e-p* correlation functions are the constant energy functions. For all studied quantities, we make contact with the experimental data.[6,22] We emphasize the importance of the state dependence of the *e-p* correlation functions for all positron annihilation characteristics. Moreover, we discuss the influence of the *e-p* interaction on the positron charge distribution, and study the effect of the resulting positron wavefunction on all quantities of interest. Also, the contribution of individual annihilation-active bands to EMD, and $\rho(\mathbf{p})$ is thoroughly analyzed.

The paper is organized as follows. In Sec. II we describe the formalism and provide details on the calculations. The results are presented and discussed in Sec. III, and in Sec. IV we conclude the paper.

II. THEORY

A. EMD and annihilation characteristics

The electronic structure of solids, required as an input to the calculation of positron annihilation characteristics, is usually calculated within the local density approximation to density-functional theory.[23] In the present calculations, the self-consistent electronic structure of bulk Si has been obtained using the linear muffin-tin orbital (LMTO) method with the atomic sphere approximation (ASA).[24] For core electrons the frozen-core approximation has been implemented. The electron wave functions $\psi_i^e(\mathbf{r}_e)$ and the charge density $n(\mathbf{r}_e)$ at the electron position $\mathbf{r}_e$, consisting of core n_c and valence n_v contributions, define both the *e-p* momentum density and annihilation rates. For periodic solids, the electron wave functions, $\psi_i^e(\mathbf{r}_e)$, may be labeled by the Bloch vector $\mathbf{k}$ and band index j, namely, $i = \mathbf{k}j$.

The electron momentum density $\rho^{EMD}(\mathbf{p})$ and the *e-p* momentum density $\rho(\mathbf{p})$ are determined, respectively, by[1]

$$\rho^{EMD}(\mathbf{p}) = \frac{1}{\Omega} \sum_{i_{occ}} \left| \int_{\Omega} e^{-i\mathbf{p}\cdot\mathbf{r}_e} \psi_i^e(\mathbf{r}_e) d\mathbf{r}_e \right|^2 \tag{1}$$

and

$$\rho(\mathbf{p}) = \sum_{i_{occ}} \left| \int_{\Omega} e^{-i\mathbf{p}\cdot\mathbf{r}_p} \psi_+(\mathbf{r}_p) \psi_i^e(\mathbf{r}_p) \sqrt{\gamma_i(\mathbf{r}_p)} d\mathbf{r}_p \right|^2, \tag{2}$$

where $\mathbf{p}$ is the electron momentum in the extended zone scheme, $\psi_+(\mathbf{r}_p)$ is the wave function of a thermalized positron (at position $\mathbf{r}_p$) in the Bloch state of $\mathbf{k}_+ = \mathbf{0}$ and $j = 1$, and Ω is the volume of the sample. The summations in Eqs. (1) and (2) are over all occupied electron states i. The functions $\gamma_i(\mathbf{r}_p)$ are the state-dependent two-particle *e-p* correlation functions, defined as the ratio of perturbed to unperturbed electron densities in the initial state i at the positron position $\mathbf{r}_p$.

The positron wave function $\psi_+(\mathbf{r}_p)$ is the solution of the Schrödinger equation, with the positron potential consisting of the external potential due to ions, the Hartree potential, and the *e-p* correlation (V_{corr}) potential.[12,25,26] The positron Hartree potential and the external potential are equal to the respective electron potentials with the opposite sign. The energy E_+ is the bottom of the positron band. The potential V_{corr}, describing the positron interaction with the electron screening cloud, can be determined from the Feynmann theorem.[12,17,25,27] For the IPM, $V_{corr}^{IPM}(\mathbf{r}_p) \equiv 0$, while within the LDA the *e-p* correlation potential is approximated by the quantity obtained for the homogeneous electron gas, namely, $V_{corr}^{LDA}(\mathbf{r}_p) = V_{corr}^{h}[n(\mathbf{r}_p)]$, parametrized in terms of the uniform electron density n_0.[25] Details on the evaluation of the WDA and GGA *e-p* correlation potentials were given in Refs. 17 and 13, respectively.

The total annihilation rate λ is defined as

$$\lambda = \pi r_0^2 c \frac{\Omega}{(2\pi)^3} \int \rho(\mathbf{p}) d\mathbf{p}$$

$$= \pi r_0^2 c \sum_t \int |\psi_+(\mathbf{r}_p)|^2 n_t(\mathbf{r}_p) \gamma_t(\mathbf{r}_p) d\mathbf{r}_p, \tag{3}$$

with r_0 and c being the classical electron radius and the velocity of light, respectively. Here t refers to different types of electrons, e.g., core or valence.

B. Enhancement factors and weighted density approximation

When a positron enters a solid, it attracts the surrounding electrons, and a polarization cloud is formed. As a result, the densities of individual electron states, *i*, at the positron position, become strongly enhanced, as compared to their initial values. In calculations of positron annihilation characteristics, this effect can be accounted for by defining the two-particle e-p correlation functions $\gamma_i(\mathbf{r}_p)$. In the IPM these correlation effects are totally neglected. In the LDA, the correlation functions $\gamma_i(\mathbf{r}_p)$ are approximated by the respective quantities for the homogeneous electron gas, $\gamma_i^h[n(\mathbf{r}_p)]$,[27] with the local electron density $n(\mathbf{r}_p)$ at the positron position $\mathbf{r}_p$. In the LDA, we can define both the state-dependent and -independent correlation functions which, however, are always local quantities. To introduce the nonlocal effects, beyond the LDA description, Barbiellini and co-workers[13,14] used a parameter-dependent GGA approach and defined the nonlocal state-independent GGA correlation functions (GGA-CEF's). For the state-dependent and nonlocal description of the correlation functions, we have used the weighted-density approximation. Since a detailed description and implementation of the WDA correlation functions were given in Ref. 17, here we only summarize the main points.

In the WDA, the e-p correlation functions have been approximated by $\gamma_t^{WDA}(\mathbf{r}_p)=\gamma_t^h[\tilde{n}_t(\mathbf{r}_p)]$, where the effective WDA electron densities $\tilde{n}_t(\mathbf{r}_p)$ have been defined for all different types t of electrons, meaning that for any t and $\mathbf{r}_p$ we have calculated the density $\tilde{n}_t(\mathbf{r}_p)$ as the solution of the charge-neutrality condition

$$\{\gamma_t^h[\tilde{n}_t(\mathbf{r}_p)]-1\}\int n_t(\mathbf{r}_e)e^{-a[\tilde{n}_t(\mathbf{r}_p)]|\mathbf{r}_e-\mathbf{r}_p|}d\mathbf{r}_e = \{\gamma_t^h[n(\mathbf{r}_p)]-1\}n_t(\mathbf{r}_p)8\pi/a_{LDA}^3[n(\mathbf{r}_p)], \quad (4)$$

with

$$a^3[\tilde{n}_t(\mathbf{r}_p)]=\frac{n_t^*(\mathbf{r}_p)\{\gamma_t^h[\tilde{n}_t(\mathbf{r}_p)]-1\}}{n_t(\mathbf{r}_p)\{\gamma_t^h[n(\mathbf{r}_p)]-1\}}a_{LDA}^3[n(\mathbf{r}_p)]$$

and

$$a_{LDA}^3[n(\mathbf{r}_p)]=8\pi\sum_t n_t(\mathbf{r}_p)\{\gamma_t^h[n(\mathbf{r}_p)]-1\}.$$

Here n_t^* and $\tilde{n}_t$ are related by

$$\tilde{n}_t(\mathbf{r}_p)=n(\mathbf{r}_p)+[n_t^*(\mathbf{r}_p)-n_t(\mathbf{r}_p)].$$

Further technical details of calculating the effective electron densities were given in Ref. 17.

The corresponding correlation functions $\gamma_t^h(n_0)$ for core and valence electrons, respectively, have been approximated by[17] $\gamma_c^h(n_0)=\epsilon(0,n_0)$[20] and $\gamma_v^h(n_0)=\gamma^h(n_0)$.[12,13,20] Here the quantities ϵ are the Kahana-like energy-dependent e-p enhancement factors, and are evaluated at the energy $E=0$ and electron density n_0.[27,28]

In the present application of the above methodology to bulk Si, we first evaluate the effective WDA electron densities according to Eq. (4). Then, for electrons of type *t*, we approximate the e-p correlation functions, appearing in Eq. (2), with the state-dependent WDA correlation functions $\gamma_i(\mathbf{r}_p)=\epsilon[E_i/E_F,\tilde{n}_t(\mathbf{r}_p)]$, where E_i is the electron eigenenergy in the initial state *i*, and E_F is the Fermi energy. For the enhancement factors $\epsilon[E,n_0]$, we have used the values calculated in Ref. 28. In the LDA–SEF approach, the quantities $\epsilon[E_i/E_F,n(\mathbf{r}_p)]$ have been substituted for the e-p correlation functions $\gamma_i(\mathbf{r}_p)$ in Eq. (2).[20]

III. RESULTS AND DISCUSSION

In this section we study in detail the influence of the positron distribution and e-p correlations on the resulting positron annihilation characteristics. Since in Si the core electrons contribution to positron annihilation is very small, in what follows we concentrate mainly on the valence electrons, but give also some results for the core electrons. We analyze the effect of different approaches to the e-p correlations on the resulting positron density distributions. Also, we discuss the importance of the nonlocal effects for the calculation of the total and partial positron annihilation rates. Moreover, the role of the state dependence of the e-p correlations is examined. To afford this, we have calculated the positron annihilation characteristics for a number of different approximations to the positron wave function and e-p correlations. Specifically, we have studied the EMD in comparison with the e-p momentum density $\rho(\mathbf{p})$, calculated within the IPM, LDA (both CEF and SEF), GGA, and WDA approaches. When calculating a given positron wave function, e.g., IPM, LDA, WDA, or GGA, the corresponding approximation for the positron correlation potential V_{corr}, occurring in the positron Schrödinger equation, has been used. Additionally, we have separated the contributions due to different annihilation-active bands to the relevant momentum densities.

As mentioned earlier, we have used the LMTO-ASA method for electronic structure calculations. According to the atomic sphere approximation, the polyhedral Wigner-Seitz cell is approximated by slightly overlapping atom centered spheres, with the total volume equal to the actual crystal volume. Since the diamond structure is an open structure, to improve its packing, an additional two empty ASA spheres have been introduced at the high-symmetry interstitial sites. For the basis functions we have used s, p, and d partial waves on both the Si and empty-sphere sites. In all calculations we have assumed an experimental lattice constant of $a=10.26$ atomic units. Moreover, in all calculations the Jarlborg–Singh (JS) correction,[29] taking into account the nonorthogonality of the plane waves in the ASA spheres, has been included when evaluating the EMD and $\rho(\mathbf{p})$, as given by Eqs. (1) and (2). However, for diamond structure the JS overlap matrix has turned out to be almost diagonal, and therefore the JS correction has not influenced substantially the calculated EMD and e-p momentum densities for silicon.

The calculated valence energy bands along three crystallographic directions in the {001} plane are shown in Fig. 1. Due to the symmetry rules, only the bands represented by solid curves contribute to the electron and e-p momentum densities. From Fig. 1(a) one can see that for momenta along the [110] direction only the first and third bands contribute to the momentum densities, while the second and fourth bands are inactive, and this holds for all Brillouin zones (BZ's). As

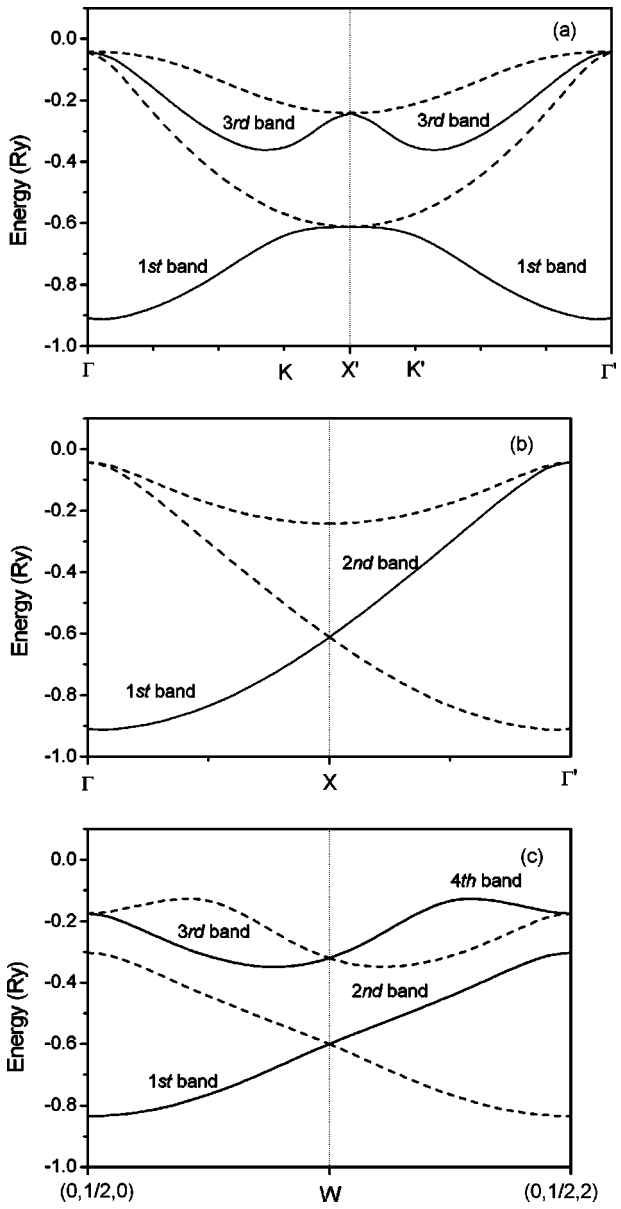

FIG. 1. Energy bands in Si along three crystallographic directions in the {001} plane. Momenta are expressed in units of $2\pi/a$. The solid curves denote the annihilation active bands, contributing to the EMD and e-p momentum densities, while the dashed curves denote the inactive bands.

can be seen in Figs. 1(b) and 1(c), the situation is different for momenta along the directions parallel to the [100] direction. The first band contributes to the momentum densities for momenta in the first BZ (1BZ), but becomes inactive in the second BZ (2BZ), while the second band, which is inactive in the 1BZ, becomes active in the 2BZ. The doubly degenerate uppermost band is inactive for the momenta along the Γ-X-Γ' line. When increasing the Jones index, then also the upper bands along the lines parallel to the [100] direction start contributing to the EMD and positron annihilation spectra. For momenta along the line starting at $(0,\pi/a,0)$ and finishing at $(0,\pi/a,4\pi/a)$ [see Fig. 1(c)], the third band interchanges with the fourth band at the **W** point, similarly to the previously mentioned interchange of the first band with the second band. Note, however, that in order to obtain 1D and 2D ACAR spectra, measured experimentally, one has to perform the planar and linear integrals of $\rho(\mathbf{p})$, respectively, which of course involves contributions from all four electron bands, since in the general points of the BZ no symmetry rules excluding some bands apply.[30] In other words, after performing 1D or 2D integration of $\rho(\mathbf{p})$, the above characteristic asymmetry of the energy bands is lost. Therefore, the dips, observed in the 1D and 2D experimental ACAR spectra for Si, would be difficult to explain in terms of the symmetry of the active bands alone.[6] This further suggests that in the interpretation of the ACAR spectra in terms of EMD, more reliable conclusions can be drawn from 3D (reconstructed) data than from ''raw'' 1D and 2D ACAR spectra. Consequently, below we present and discuss results for the calculated 3D momentum densities in bulk Si, in comparison with the 3D reconstructed experimental data of Tanigawa.[6]

A. Momentum density distributions

In Fig. 2 we present the contour plots of $\rho^{EMD}(\mathbf{p})$, $\rho^{IPM}(\mathbf{p})$, $\rho^{LDA\text{-}SEF}(\mathbf{p})$, and $\rho^{WDA}(\mathbf{p})$ in the {001} plane. These we compare with the relevant contour plots of the experimentally reconstructed 3D ACAR spectra,[6] given in Fig. 3. The experimental spectra are the raw data measured at 14 K with resolution of 0.73×0.73 mrad^2. All spectra have been normalized to unity at the maximum value in the plane. Both for the calculated momentum densities and the experiment, the contours have been plotted with the spacing of 0.04.

First thing to observe in Figs. 2 and 3 is that both LDA-SEF and WDA approaches are in very good agreement with experiment, and that they are an enormous improvement on the EMD and IPM results. This is indicative of the fact that the e-p correlations are vital for a correct interpretation of the experimental ACAR data, especially in the low-momentum region. There, similarly to the experimental curves, all calculated spectra show dips along the lines parallel to the [100] direction and in the [110] direction. One can see that when the Jones zone index is increased these dips become more and more pronounced along the [100] lines. The maximum value of the momentum density in the {001} plane is found along the [110] direction. For EMD and IPM contour plots the dips along the [110] direction are much more shallow than the one observed in the experimental spectra. When comparing the EMD and IPM results, one can see that taking into account the positron wave function leads to a slight improvement of the agreement between theory and experiment. This is in line with the earlier observation made by Panda and co-workers[7,10] Nevertheless, as already mentioned, the major improvement comes only from the e-p correlations.

Another thing to notice is that the differences between the local, LDA-SEF, and nonlocal, WDA approaches are not significant although, as can be clearly seen in Figs. 4 and 5, $\rho^{LDA\text{-}SEF}(\mathbf{p})$ is a slightly faster increasing function of momentum $\mathbf{p}$ than $\rho^{WDA}(\mathbf{p})$. In these figures we show all relevant 3D momentum densities for the same crystallographic directions as those in Fig. 1. Specifically, in Fig. 4 we compare, to the experimental ACAR spectra, the EMD and e-p momentum densities along the Γ-K-X'-K'-Γ' line, as calculated within the IPM, LDA (both CEF and SEF), GGA, and

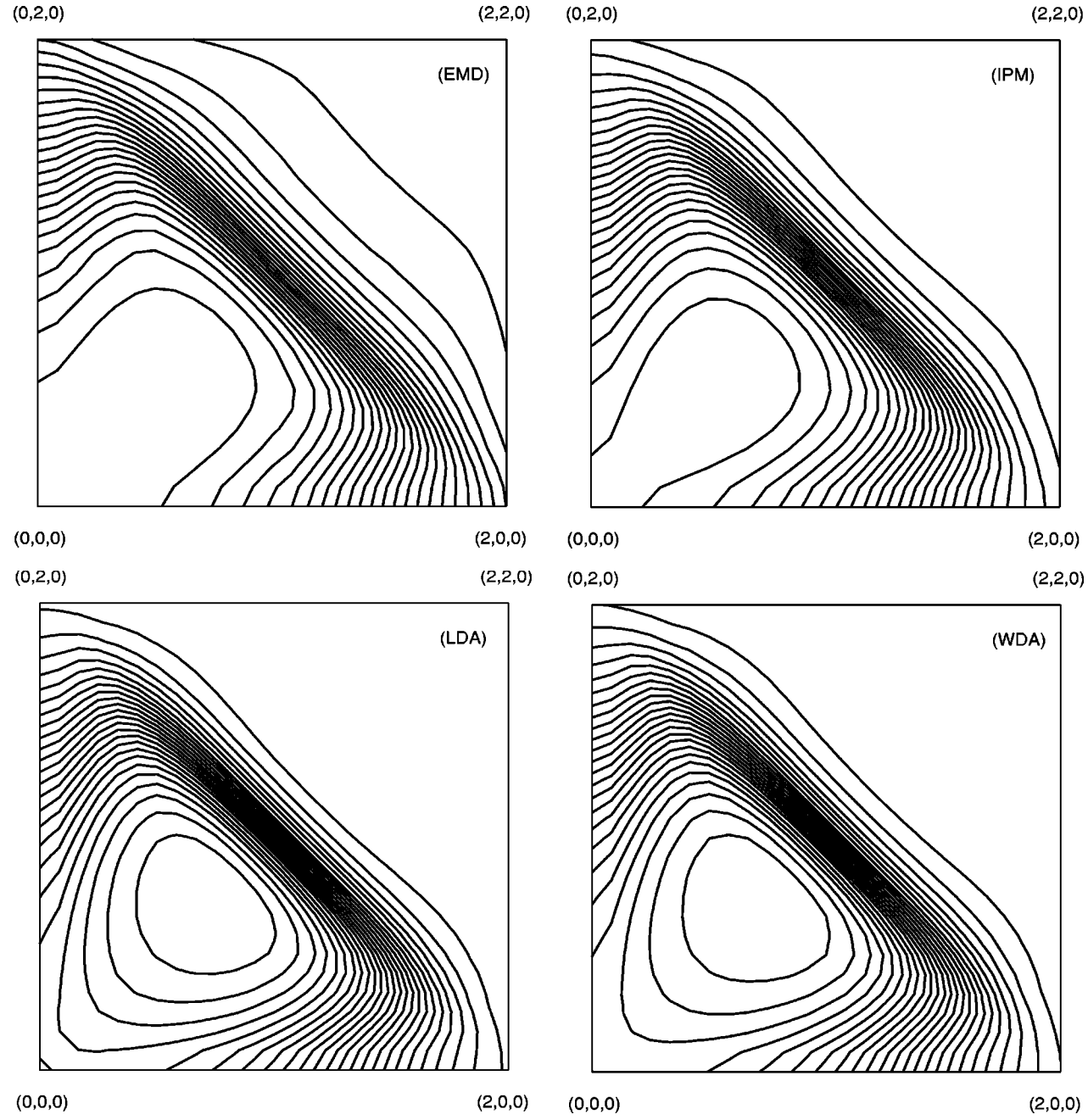

FIG. 2. Contour plots due to the EMD, IPM, LDA-SEF, and WDA approaches, for momenta **p** in the {001} plane. Momenta are expressed in units of $2\pi/a$. Spectra are normalized to unity at the maximum in the plane. The contour spacing is 0.04 to agree with the spacing of the experimental data in Fig. 3.

WDA approaches. In Fig. 5 the relevant quantities are given along the line starting at $(0,\pi/a,0)$ and finishing at $(0,\pi/a,4\pi/a)$.

One should remember that the *e-p* correlation functions $\gamma_{\mathbf{k}j}(\mathbf{r})$, determined within the LDA-SEF and WDA approaches, are state dependent, and they are increasing functions of the electron energy $E_{\mathbf{k}j}$. Other approaches, like the LDA-CEF and GGA, are state independent, and, as can be seen in Figs. 4 and 5, cannot reproduce the experimentally observed rise of the *e-p* momentum density when approaching the Jones zone face. Looking at the GGA curve, including some form of nonlocality, and comparing it to the results of the LDA-CEF approach, one can observe that both of these approaches lead to nearly constant enhancement factors, $\epsilon(\mathbf{p})$, with the GGA curve rising slightly faster with momentum than the LDA-CEF curve, possibly reflecting the yinfluence of nonlocal effects. Further comparing the WDA and LDA-SEF curves, one can see that the latter curve is a more quickly increasing function of momentum than the WDA curve, and that the nonlocal effects are not very important. Nevertheless, the effect of nonlocality is different for state-dependent and -independent quantities, but it is the state dependence that is vital for comparison with the experimental data. The state dependence of the *e-p* correlation functions leads to a considerable improvement of the agreement between theory and experiment, as compared to the state-independent LDA-CEF and GGA approaches. For momenta **p** in the 1BZ, both LDA-SEF and WDA momentum

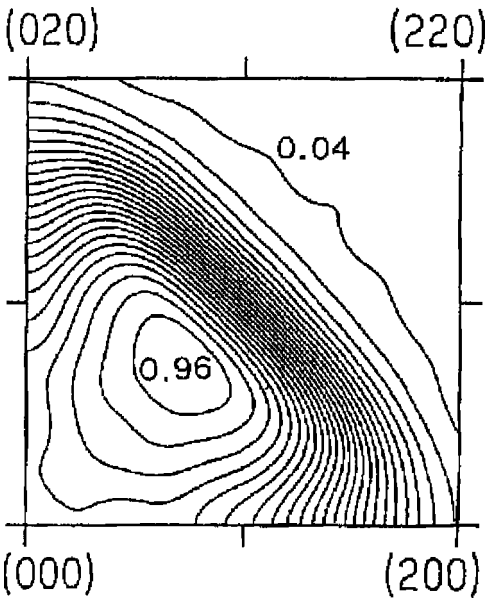

FIG. 3. Contour plots of the 3D reconstructed experimental data of Ref. 6 for momenta **p** in the {001} plane. Momenta are expressed in units of $2\pi/a$. Spectra are normalized to unity at the maximum in the plane. The contour spacing is 0.04.

densities reproduce the experimental spectra quite well. From Fig. 5 one can see that for momenta along the $(0,\pi/a,0)-W$ line the agreement between $\rho^{WDA}(\mathbf{p})$ and the experiment is excellent. For momenta along the Γ-K line (see Fig. 4), it is difficult to decide whether the LDA-SEF or WDA approach is better. However, in the low-momentum region, the slope of the characteristic dip of $\rho^{WDA}(\mathbf{p})$ follows nearly exactly the experimental slope, while close to the K points the LDA-SEF approach provides better results. One can say that the effect of e-p correlations is stronger in the LDA-SEF approach, and that the WDA approach leads to more averaged quantities.

For the high-momentum region a negative slope of the e-p momentum densities is observed. However, these are only the LDA-SEF and WDA curves, which intersect the experimental spectra at about half of their maximum height. Taking into account a finite experimental resolution (marked in Figs. 4 and 5), we can conclude that the state dependence of the e-p correlations improves the agreement between the theory and experiment, as compared with IPM, LDA-CEF, and GGA approaches. Note that for higher momenta **p**, the EMD approach reproduces the shape of the experimental ACAR spectra surprisingly well, much better than the IPM, LDA-CEF, and GGA approaches. Finally, it should be pointed out here that, in the experimental spectra, large tails are seen along the K'-Γ' line in the high-momentum region. Such tails should not be attributed to the core electrons, since in Si their contribution to the positron annihilation is very small.[17] This statement is reinforced by Fig. 6, where we show, as a function of momentum, the ratio of the calculated core electron momentum distribution, $\rho_{core}(\mathbf{p})$, to the total value of the e-p momentum distribution, $\rho(\mathbf{p})+\rho_{core}(\mathbf{p})$, at $\mathbf{p}=0$, for IPM, LDA, and WDA approaches. It can be seen that the e-p correlations further reduce the already small core electron contribution to the total e-p momentum distribution, as calculated within the IPM approach. Note that correlations

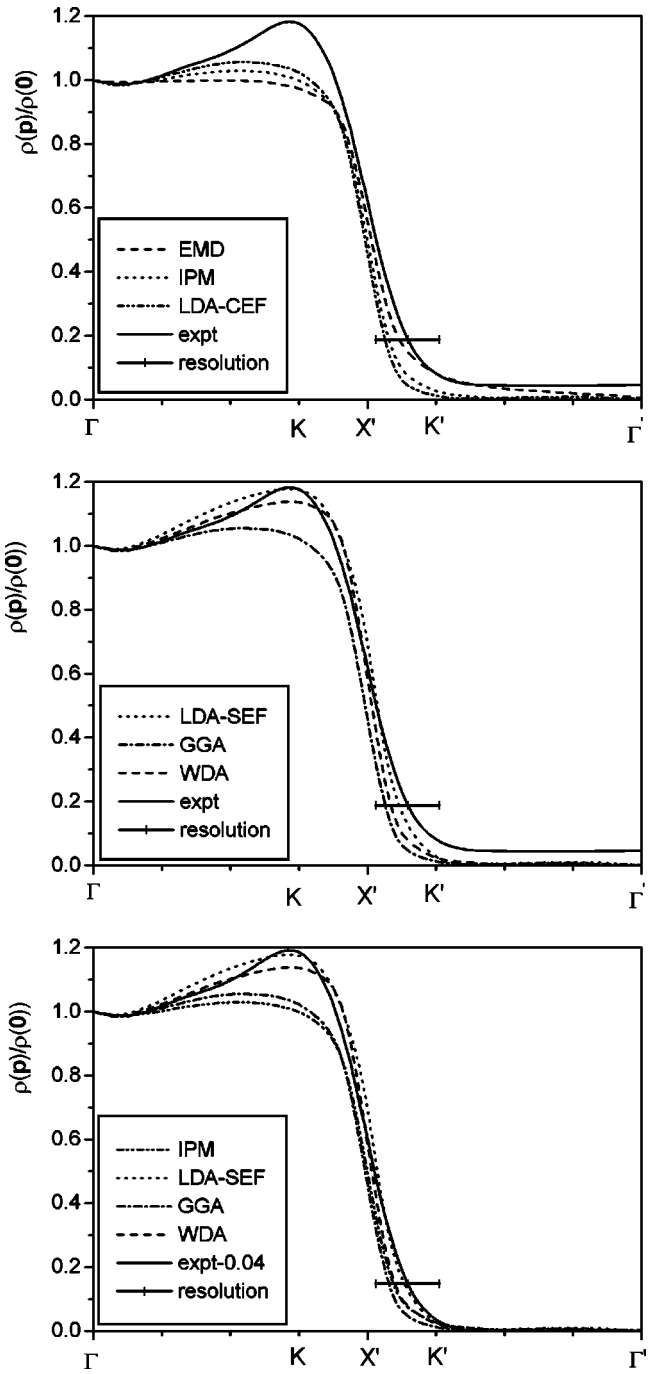

FIG. 4. Momentum densities calculated within various approaches and compared to the experimental data for momenta **p** along the [110] direction. Spectra are normalized to unity at $\mathbf{p}=\mathbf{0}$.

due to the valence electrons are what matters here. Consequently, it seems justified to assume that the constant tails in the experimental data are due to a constant background of the raw ACAR data. As a result, for comparison with the present calculations, in Figs. 4 and 5 we have subtracted this constant background from the experimental spectra. This subtraction does not influence the comparison between theory and experiment, except at the high-momentum region, where all calculations show much better agreement with experiment.

Let us look in detail at the band-by-band decomposed momentum densities along the Γ-X-Γ' line (the [100] direc-

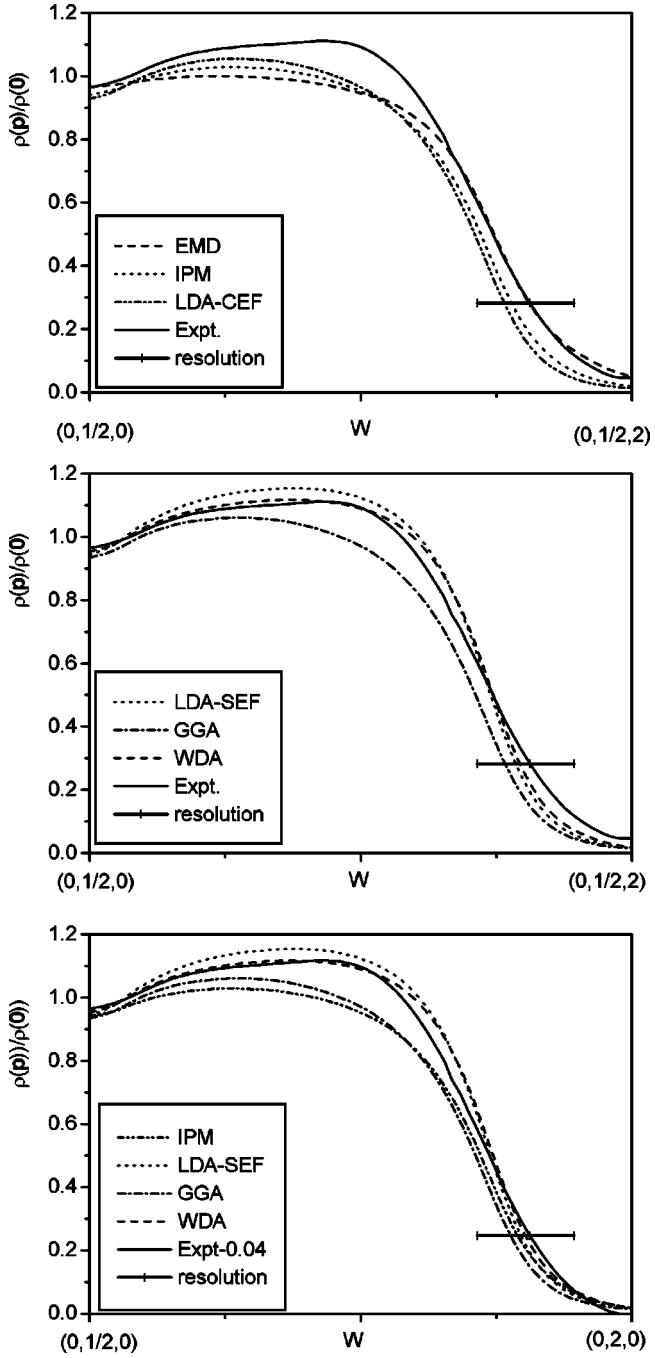

FIG. 5. Momentum densities calculated within various approaches and compared to the experimental data for momenta **p** along the line parallel to the [100] direction in the {001} plane. Momenta are expressed in units $2\pi/a$. Spectra are normalized to unity at $\mathbf{p}=0$.

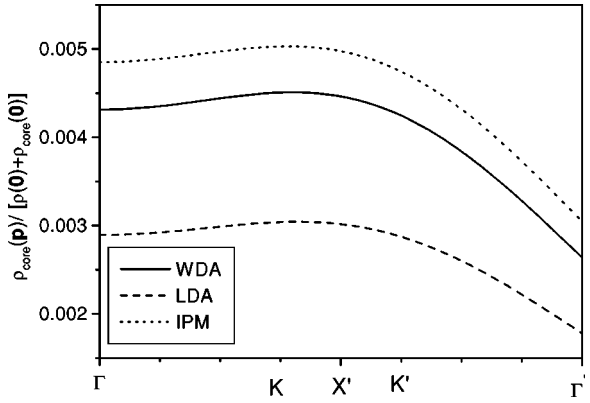

FIG. 6. The momentum dependence of the calculated ratios of the core electron to total e-p momentum distribution at $\mathbf{p}=0$ for IPM, LDA, and WDA approaches. All curves are normalized in the same way as those for the valence electron momentum densities, shown in Figs. 4 and 5. That is, the value of total momentum distribution, $\rho(\mathbf{p})+\rho_{core}(\mathbf{p})$, at $\mathbf{p}=0$, is set equal to unity.

tion), as shown in Fig. 7, and for the Γ-K-X-K'-Γ' and $(0,\pi/a,0)$–W–$(0,\pi/a,4\pi/a)$ lines, respectively, as presented in Figs. 8 and 9. In contrast to all other directions, the momentum densities along the Γ-X-Γ' line are decreasing functions of momentum **p** . As can be seen in Fig. 7, in the [100] direction only the first and second bands contribute to the momentum densities, and these contributions are decreasing functions of momentum, possibly reflecting spatial localization of the electron distribution, away from the positron position. Also, in other directions the first and second band contributions decrease with momentum (see Figs. 8 and 9). However, the third and fourth band contributions increase sharply before falling toward the Jones zone face. It is the third and fourth bands that give rise to the hump in the LDA-SEF and WDA momentum density curves. Here the shape of the momentum densities is a combined effect of the individual band contributions, where the third and fourth bands reflect the strong energy dependence of the corresponding correlation functions. From Figs. 8 and 9, it can be seen that the negative slope of the momentum densities is characteristic of lower, first and second, electron bands. The electron density is so strongly varying a function, especially in the interstitial region, where the positron is found, that the **r** dependence of the e-p correlation functions, $\gamma_{\mathbf{k}j}(\mathbf{r})$, dominates over their energy, $E_{\mathbf{k}j}$ dependence. Except for the momenta falling very close to the Γ point, the (normalized) WDA and LDA-SEF momentum densities are intermediate between the EMD and IPM approaches. Close to the Γ point, the WDA and LDA-SEF enhancement factors are decreasing functions of momentum **p**, and a small dip is seen in both spectra for momenta close to zero. Also, very close to the Γ' point, in the 2BZ, the WDA and LDA-SEF enhancement

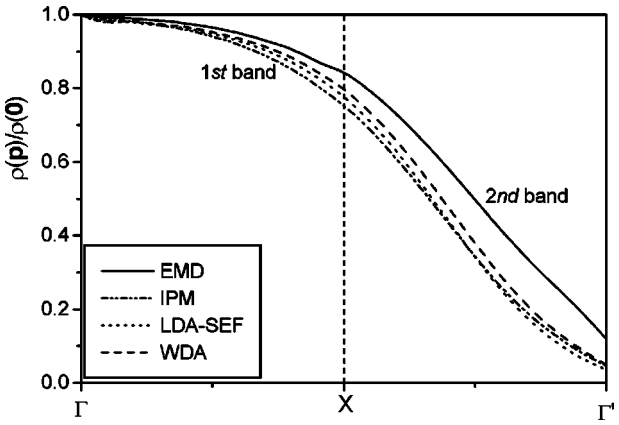

FIG. 7. Momentum densities calculated within the EMD, IPM, LDA-SEF, and WDA approaches, for momenta **p** along the [100] direction. Spectra are normalized to unity at $\mathbf{p}=0$.

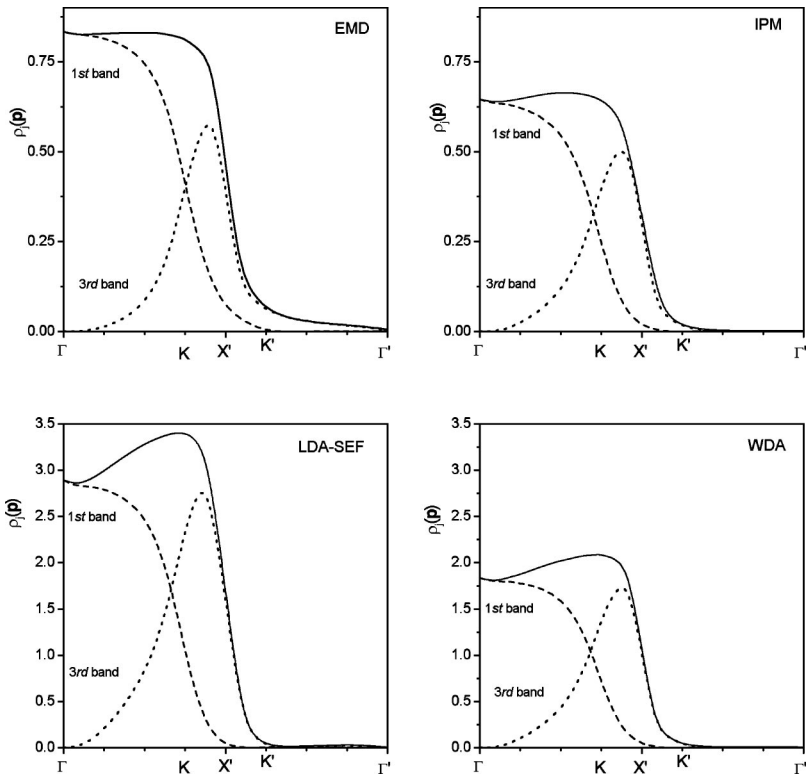

FIG. 8. Momentum densities calculated within the EMD, IPM, LDA-SEF, and WDA approaches, for momenta **p** along the [110] direction. The total curves are decomposed into the contributions from the first (dashed line) and third (dotted line) bands.

factors show a negative slope as a function of momentum. This effect could be attributed to localization of electrons along the tetrahedral bonds. Finally, note that due to the strong localization of the positron in the interstitial region, in the [100] direction the effect of the positron distribution is stronger than the *e-p* correlation effects.

Before leaving this subsection let us discuss the core electron contribution to the total 1D *e-p* momentum densities for Si. To facilitate a comparison with experiment, in Fig. 10 (top panel) we show our calculated positron annihilation probability densities,

$$P(p_z)=2\pi\int_{|p_z|}^{\infty} p\rho_{core}(|\mathbf{p}|)dp,$$

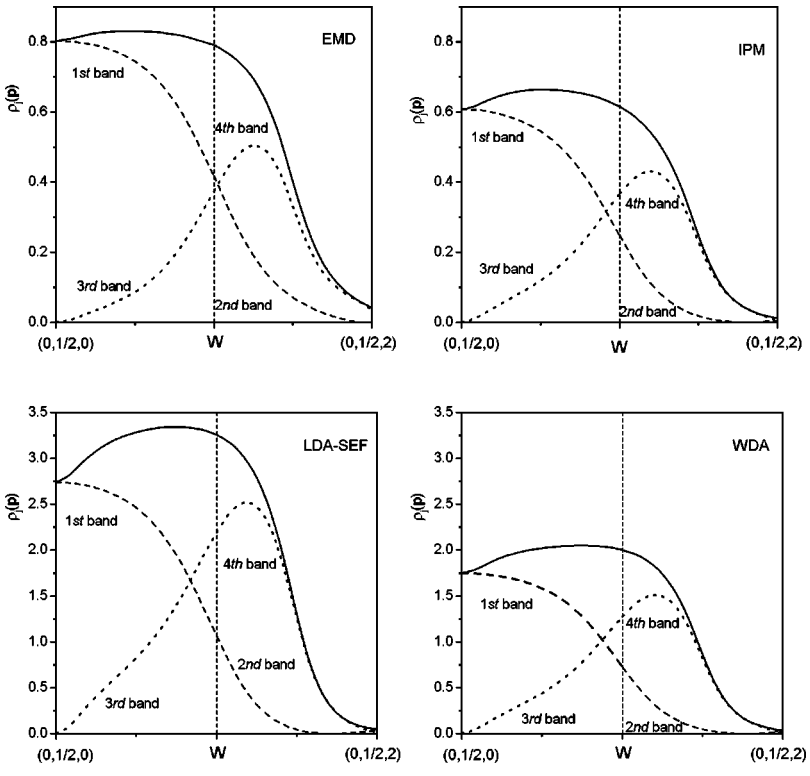

FIG. 9. Momentum densities calculated within the EMD, IPM, LDA-SEF, and WDA approahces, for momenta **p** along the line parallel to the [100] direction in the {001} plane. Momenta are expressed in units of $2\pi/a$. The total curves are decomposed into the contributions from the first, second (dashed lines), third, and fourth (dotted lines) bands.

for IPM, LDA, and WDA approaches, with the experimental data obtained by scan from Ref. 14. Additionally, in the bottom panel of this figure, we include a complete set of experimental and theoretical results for Si from the latter reference (see Fig. 3 of that reference). Here the theoretical curves correspond to IPM, LDA, and GGA approahces. The thing to note, when comparing the theoretical results in both panels of Fig. 10, is that both IPM curves are very similar. What is also encouraging is that although the theoretical curves in the top panel of the figure have not been convoluted with a Gaussian, to account for the experimental resolution function, the agreement of the WDA curve with the experimental data is quite satisfactory. That our LDA curve runs lower than the data, and as compared to the LDA curve in the bottom panel, is an effect of the form of the positron wave function. This can easily be seen in Fig. 11, where we have plotted the theoretical curves $P_{core}^{IPM}(p_z)$ for positron wave

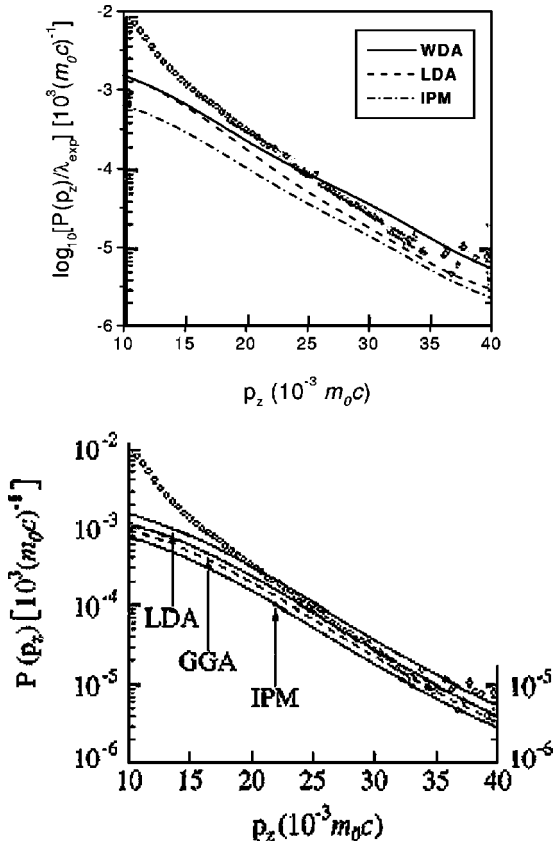

FIG. 10. Positron annihilation probability densities $P(p_z)$ for bulk Si, from the present calculations for IPM, LDA, and WDA approaches, in comparison with the experimental data extracted by scan from the paper by Alatalo *et al.* [Phys. Rev. B **54**, 2397 (1996)] (top panel). The theoretical curves have not been convoluted with a Gaussian, meant to mimic the experimental resolution. Since the experimental Doppler broadering data for bulk Si of Alatalo *et al.* have been normalized to unit volume, our theoretical curves for the core electrons have been normalized to $\lambda_{core}/\lambda_{expt}$, where $\lambda_{expt}=1/218\ \text{ps}^{-1}$ has been taken from Alatalo *et al.* In the bottom panel of the figure, both the measured data, and the theoretical results for Si for IPM, LDA, and GGA approaches, from the above reference (see Fig. 3 of that reference) are shown. The theoretical results have been convoluted with a Gaussian. The two different GGA curves are due to LMTO-ASA (solid curve) and the atomic superposition band-structure methods (dashed curve).

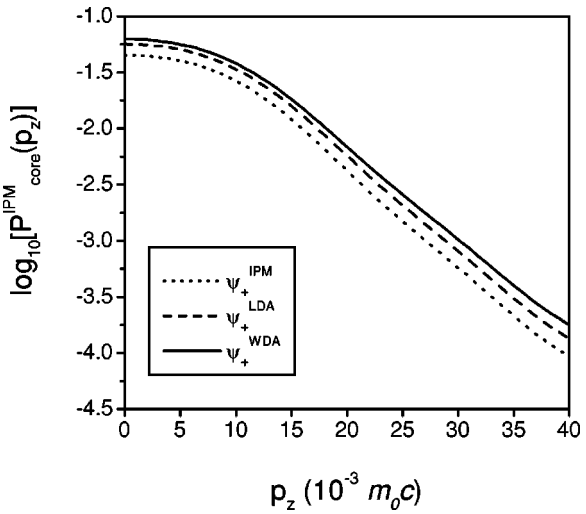

FIG. 11. The momentum dependence of the positron annihilation probability density $P(p_z)$ for bulk Si, calculated within the IPM approach for different positron wave functions.

functions obtained with IPM, LDA, and WDA correlation potentials. The shape of the curves is similar, but the values, although very small, differ quite noticeably from one another. Apart from Fig. 11, from Table I one can also see that the calculated core electron contributions to the total annihilation rates are strongly dependent on the positron wave function used in the calculations. The largest values, at a given positron wave function, are due to the LDA, meaning that the nonlocal effects reduce the core electron contribution to the total annihilation rate. Finally, the difference between the present LDA calculation for the core electrons, as compared to the one of Ref. 14, is also partially due to the fact that, when calculating correlation functions, we have assumed the enhancement factors to be $\epsilon(0,r_s)$, while Alatalo *et al.*[14] assumed correlation functions $\gamma^h(r_s)$ which are approximately equal to $\epsilon(0.64,r_s)$.

Summarizing the results of this section, it can be said that the WDA approach works well for all positron annihilation characteristics calculated here for bulk Si. In line with what has already been said, the satisfactory agreement with experiment reflects the paramount importance of the *e-p* correlation effects in the first place, but nonlocal effects also play a role here.

B. Effect of positron distribution on positron annihilation characteristics

The *e-p* correlation effects are also seen in the positron distribution, through the *e-p* correlation potentials used in

TABLE I. The core annihilation rates ($\times 10^9\ \text{s}^{-1}$) for bulk Si, calculated for different theoretical approaches according to Eq. (3). The superscripts in λ specify the approximation used for the *e-p* correlation functions $\gamma_t(\mathbf{r})$, and superscripts in ψ_+ correspond to the type of the *e-p* correlation potential, used in the positron Schrödinger equation. The value of λ_{core}^{GGA} is taken from Ref. 13.

	ψ_+^{IPM}	ψ_+^{LDA}	ψ_+^{WDA}
λ_{core}^{IPM}	0.060	0.076	0.086
λ_{core}^{LDA}	0.113	0.142	0.158
λ_{core}^{GGA}		0.110	
λ_{core}^{WDA}	0.101	0.128	0.143

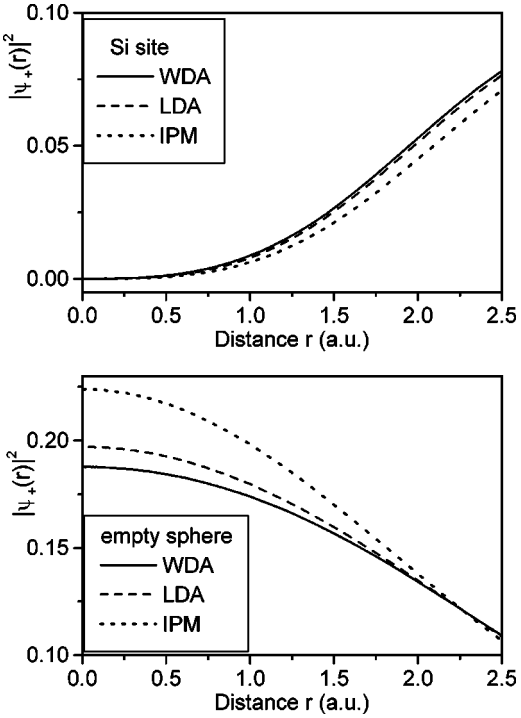

FIG. 12. Positron density distribution as calculated within various approximations for the *e-p* correlation potential as a function of distance **r** from the center of the Si ASA (upper panel) and the empty sphere (lower panel).

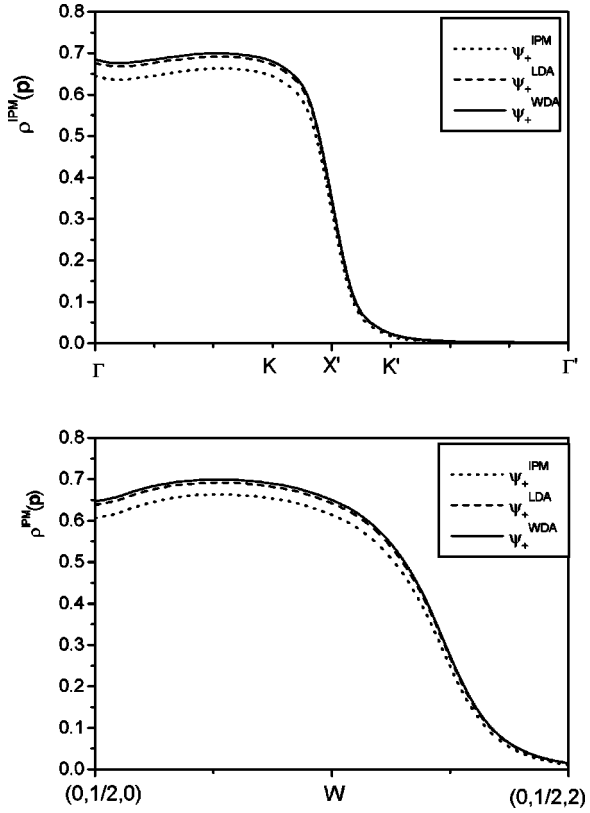

FIG. 13. The IPM momentum density, calculated according to Eq. (2) for different positron wave functions, shown in Fig. 9, for momenta along [110] and (0,1/2,0) to (0,1/2,2) directions. Momenta are expressed in units of $2\pi/a$.

the positron Schrödinger equation. The corresponding positron distributions $|\psi_+^{WDA}(\mathbf{r})|^2$ and $|\psi_+^{LDA}(\mathbf{r})|^2$, relative to the IPM distribution, are shown in Fig. 12. As mentioned earlier, to improve the packing of the diamond structure, in the electronic structure calculations with the LMTO-ASA method, two empty spheres have been included. As can be seen in Fig. 12, it is in the empty spheres that the positron distribution has the highest weight (about 75%). Electron-positron correlations shift the weight of the positron distribution from the interstitial region (represented here by the empty spheres) toward the Si site. This effect, observed both for LDA and WDA appraoches, is easy to understand, since the ''dressed'' positron is more neutral to ions. Nonlocality of the *e-p* correlations enhances the above redistribution of $|\psi_+(\mathbf{r})|^2$ in the Wigner-Seitz cell, as compared to the LDA approach. The explanation is that positron is mainly screened by the valence electrons, which are found with the highest probability at the Si sites. Within the WDA approach, positron follows its screening cloud,[17] moving toward the Si atoms.

Let us now concentrate on the influence of the positron wave function on the *e-p* momentum densities and positron annihilation rates. For this we start with the discussion of the IPM results, because they contain unperturbed information on the overlap of the electron and positron wave functions. In Fig. 13, the effect of the positron distribution on the IPM momentum density is shown for two crystallographic directions in the {001} plane. One can see that including the *e-p* correlation potential in the positron Schrödinger equation increases the overlap of the positron wave function with the electron wave functions. Concerning the momentum dependence of $\rho^{IPM}(\mathbf{p})$ in the 1BZ, it is only very slightly affected by the positron distribution. The nonlocality of $V_{corr}(\mathbf{r})$ does not change the IPM momentum density very much, as compared with the case of the LDA positron wave function.

The effect of V_{corr} is even more pronounced in the Lock-Crisp-West (LCW) folded IPM momentum density[31]

$$\rho_j^{IPM}(\mathbf{k}) = \sum_G \rho_j^{IPM}(\mathbf{k}+\mathbf{G}) = \int_\Omega |\psi_{\mathbf{k}j}(\mathbf{r})|^2 |\psi_+(\mathbf{r})|^2 d\mathbf{r},$$

where **G** are the reciprocal-lattice vectors. The results for the four bands along the $(0,\pi/a,0)$ to $(0,\pi/a,2\pi/a)$ line are presented in Fig. 14. Note that the LCW momentum densities also contain information on the high-momentum components of the ACAR spectra. The effect of the *e-p* correlations is most pronounced in the fourth, highest, occupied band. Here the nonlocality of the *e-p* correlations does not seem to be of vital importance.

C. Positron lifetime

A good test of the quality of any approach is the calculated value of the positron lifetime. In Table II we present the positron lifetimes for bulk Si, calculated for different approximations with respect to the positron wave function and the *e-p* correlations. Looking at the second row of the table, one can see that the shape of the positron wave function has a substantial influence on the resulting IPM positron lifetimes. The IPM positron wave function gives rise to longer positron lifetime than is the case for the LDA and WDA approaches. The nonlocality of the *e-p* correlations in the positron correlation potential substantially increases the total

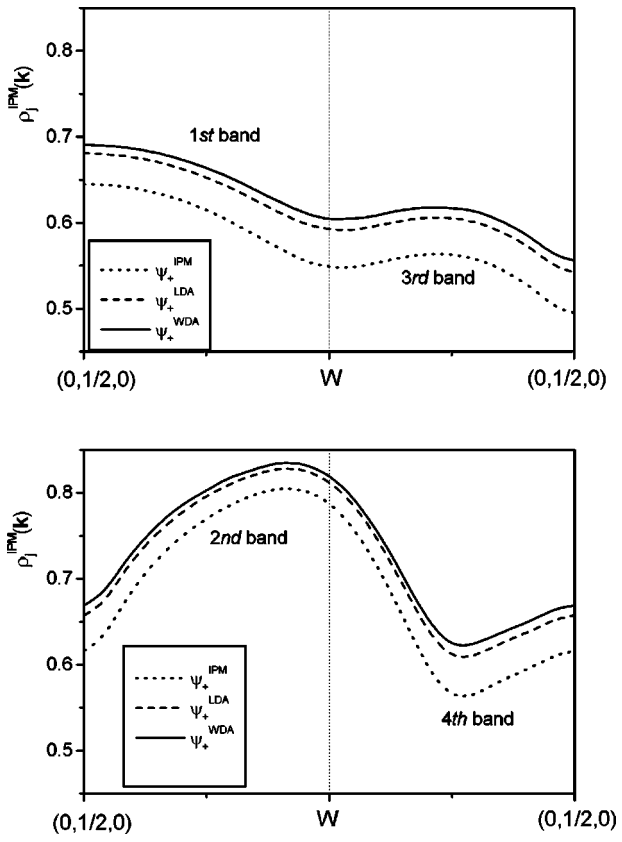

FIG. 14. Contribution of different occupied electron bands to the downfolded IPM momentum density, calculated for different positron wave functions, shown in Fig. 9, for momenta along the (0,1/2,0) to (0,1/2,2) direction. Momenta are expressed in units of $2\pi/a$.

annihilation rate, λ $(=1/\tau)$, as compared to the LDA. For the positron lifetime the present calculations give the best agreement with the experimental value of 217 ± 2 ps (Ref. 22) in two cases: first, within the WDA approach with the WDA positron wave function; and second, within the LDA approach with the IPM positron wave function. In the second case, the LDA values of the correlation functions, $\gamma_t(\mathbf{r})$, have been used, but the *e-p* correlation potential V_{corr} has been neglected in the positron Schrödinger equation. Although giving a better agreement with experiment, the second approach violates Feynmann's theorem, relating the *e-p* correlation potential to the distribution of the screening electron cloud surrounding the positron. Therefore, the WDA value is considered to be in the best agreement with the experimental value. This gives us confidence concerning the application of the WDA approach to calculations of the *e-p* momentum densities and annihilation rates, in other semiconductors, and also for studying defects and vacancies.

IV. CONCLUSIONS

Summarizing the results of the present paper, it should be stressed that *e-p* correlations are absolutely essential for obtaining good agreement of the calculated and experimental momentum densities in silicon. It is the state dependence of the *e-p* correlation functions, whether local or nonlocal, that plays the most significant role here. Except for the momenta along the [100] direction, the effect of the positron distribution on the resulting ACAR spectra is much less important. Also, the nonlocal effects are not crucial for the *e-p* momentum densities; however, they are vital for the evaluation of the positron lifetime. This follows from the fact that it is not the difference in the shape of the WDA and LDA-SEF curves which matters, but their magnitude. That the nonlocal effects do not matter too much can also be seen when comparing the state-independent, i.e., LDA-CEF and GGA, results. Further support for the importance of the state dependence of the correlation functions, as opposed to the nonlocality, is provided by a comparison of the WDA and GGA momentum densities, although both of these approaches include the nonlocal effects in a different way. Nevertheless, the GGA does not reproduce the characteristic hump close to the Jones zone face. Finally, these calculations show that to obtain good agreement with experiment, both the state-dependent correlation functions and positron wave function have to be correctly incorporated into calculations of the positron annihilation characteristics in silicon. Therefore, for any study of the electronic properties of perfect or defective semiconductors, neither IPM nor state-independent approaches would be satisfactory. As for the possible future application of the present methodology to study defects in semiconductors, both the LMTO-ASA and WDA approaches are general enough to be extended to such systems. In fact, the intention of the present authors is to reach this goal in the long run, and this is why the present study was undertaken in the first place. However, one has to be careful with respect to calculating the effective charge densities n_t to obtain the corrrect momentum distributions.[17] Therefore, for supercells of defective semiconductors, that part of the implementation will need additional effort and modifications.

TABLE II. Positron lifetimes (in picoseconds) for bulk Si, calculated for different approximations. The superscripts in τ specify the approximation used for the *e-p* correlation functions $\gamma_t(\mathbf{r})$, and superscripts in ψ_+ correspond to the type of the *e-p* correlation potential, used in the positron Schrödinger equation. The value of τ^{GGA} is taken from Ref. 13.

	ψ_+^{IPM}	ψ_+^{LDA}	ψ_+^{WDA}
τ^{IPM}	1005	936.7	914.3
$\tau^{LDA\text{-}CEF}$		210.5	
τ^{GGA}		210	
$\tau^{LDA\text{-}SEF}$	219.3	211.7	209.2
τ^{WDA}	229.4	220.0	217.0

ACKNOWLEDGMENTS

We would like to thank Thomas Jarlborg and Grażyna Kontrym-Sznajd for helpful discussions, and Maciej Kazimierski for technical assistance. We are grateful to the Royal Society (U.K.) and the State Committee for Scientific Research (Poland) (Grant No. 2P03B 107 16) for financial support of this work.

*Electronic address: ania@highscreen.int.pan.wroc.pl
†Electronic address: Z.Szotek@dl.ac.uk
‡Electronic address: W.M.Temmerman@dl.ac.uk

[1] For a review see, e.g., R. N. West, *Positron Studies of Condensed Matter* (Taylor and Francis, London, 1974); S. Berko, in *Positron Solid State Physics*, edited by W. Brandt and A. Dupasquier (North-Holland, Amsterdam, 1983), p. 64; M. J. Puska and R. M. Nieminen, Rev. Mod. Phys. **66**, 841 (1994); R. M. Nieminen, in *Positron Spectroscopy of Solids*, edited by A. Dupasquier and A. P. Mills, Jr. (IOS Press, Amsterdam, 1995), p. 443.

[2] J. C. Erskine and J. D. McGervey, Phys. Rev. **151**, 615 (1966); A. A. Shulman, G. M. Beardsley, and S. Berko, Appl. Phys. **5**, 367 (1975); R. N. West, J. Mayers, and P. A. Walters, J. Phys. E **14**, 478 (1981); W. Liu, S. Berko, and A. P. Mills, Jr., Mater. Sci. Forum **105-110**, 743 (1992).

[3] D. Stroud and H. Ehrenreich, Phys. Rev. **171**, 399 (1968).

[4] K. Fujiwara, T. Hyodo, and J. Ohyama, J. Phys. Soc. Jpn. **33**, 1047 (1972); K. Fujiwara and T. Hyodo, *ibid.* **35**, 159 (1973).

[5] M. J. Puska, S. Mäkinen, and R. M. Nieminen, Phys. Rev. B **39**, 7666 (1989); C. Penetta, Solid State Commun. **77**, 159 (1991).

[6] M. Saito, A. Oshiyama, and S. Tanigawa, Phys. Rev. B **44**, 10 601 (1991); S. Tanigawa, Mater. Sci. Forum **105-110**, 493 (1992); S. Tanigawa, in *Positron Spectroscopy of Solids* (Ref. 1), p. 729.

[7] B. K. Panda and D. P. Manhapadra, J. Phys.: Condens. Matter **5**, 3475 (1993); B. K. Panda, Phys. Rev. B **49**, 2521 (1994).

[8] Z. Tang, M. Hasegawa, T. Chiba, M. Saito, H. Sumiya, Z. Q. Li, T. Akahane, Y. Kawazoe, and S. Yamaguchi, Mater. Sci. Forum **255-257**, 411 (1997); Phys. Rev. Lett. **78**, 2236 (1997).

[9] M. Saito and A. Oshiyama, Phys. Rev. B **53**, 7810 (1996); B. K. Panda, S. Fung, and C. D. Beling, *ibid.* **53**, 1251 (1996).

[10] B. K. Panda, S. Fung, and C. D. Beling, Mater. Sci. Forum **255-257**, 179 (1997); **255-257**, 575 (1997).

[11] M. Saito, Z. Tang, T. Chiba, and M. Hasegawa, Mater. Sci. Forum **255-257**, 184 (1997).

[12] R. M. Nieminen and M. J. Puska, Phys. Rev. Lett. **50**, 281 (1983); R. M. Nieminen, M. J. Puska, and M. Manninen, *ibid.* **53**, 1298 (1984); M. J. Puska and R. M. Nieminen, J. Phys. F: Met. Phys. **13**, 2695 (1983).

[13] B. Barbiellini, M. J. Puska, T. Torsti, and R. M. Nieminen, Phys. Rev. B **51**, 7341 (1995); B. Barbiellini, M. J. Puska, T. Korhonen, A. Hajru, T. Torsti, and R. M. Nieminen, *ibid.* **53**, 16 201 (1996); B. Barbiellini, M. Hakala, M. J. Puska, and R. M. Nieminen, *ibid.* **56**, 7136 (1997).

[14] M. Alatalo, B. Barbiellini, M. Hakala, H. Kauppinen, T. Korhonen, M. J. Puska, K. Saarinen, P. Hautojärvi, and R. M. Nieminen, Phys. Rev. B **51**, 4176 (1995); M. Alatalo, H. Kauppinen, M. J. Puska, K. Saarinen, J. Mäkinen, P. Hautojärvi, and R. M. Nieminen, *ibid.* **54**, 2397 (1996).

[15] P. Asoka-Kumar, M. Alatalo, V. J. Gosh, A. C. Kruseman, B. Nielsen, and K. G. Lynn, Phys. Rev. Lett. **77**, 2097 (1996); J. Kuriplach, T. Van Hoede, B. Van Waeyenberge, C. Dauwe, D. Seegers, N. Balcaen, A. L. Morales, M. A. Trauwaert, J. Vanhellewmont, and M. Šob, Mater. Sci. Forum **255-257**, 605 (1997).

[16] N. Sakai, N. Shiotani, P. Iroh, O. Mao, M. Ito, H. Kawasara, Y. Ameniya, and M. Ando, J. Phys. Soc. Jpn. **58**, 3270 (1989).

[17] A. Rubaszek, Z. Szotek, and W. M. Temmerman, Phys. Rev. B **58**, 11 285 (1998).

[18] G. Kontrym-Sznajd and A. Rubaszek, Phys. Rev. B **47**, 6950 (1993); **47**, 6960 (1993).

[19] S. M. Kim and A. T. Stewart, Phys. Rev. B **11**, 2490 (1975); T. Hyodo, T. McMullen, and A. T. Stewart, in *Positron Annihilation*, edited by P. G. Coleman, S. C. Sharma, and L. M. Diana (North-Holland, Amsterdam, 1982), p. 201; P. Kubica and A. T. Stewart, Phys. Rev. Lett. **34**, 852 (1975).

[20] S. Daniuk, G. Kontrym-Sznajd, A. Rubaszek, H. Stachowiak, J. Mayers, P. A. Walters, and R. N. West, J. Phys. F: Met. Phys. **17**, 1365 (1987); S. Daniuk, M. Šob, and A. Rubaszek, Phys. Rev. B **43**, 2580 (1991).

[21] P. E. Mijnarends and R. M. Singru, Phys. Rev. B **19**, 6038 (1979); M. Šob, J. Phys. F: Met. Phys. **12**, 571 (1982).

[22] A. Seeger, F. Banhart, and W. Brauer, in *Positron Annihilation*, edited by L. Dorikens-Vanpraet, M. Dorikens, and D. Segers (World Scientific, Singapore, 1989) p. 275, and references cited in Ref. 9.

[23] P. Hohenberg and W. Kohn, Phys. Rev. **136**, B364 (1964); W. Kohn and L. J. Sham, Phys. Rev. **140**, A133 (1965).

[24] O. K. Andersen, Phys. Rev. B **12**, 3060 (1975); W. R. L. Lambrecht and O. K. Andersen, *ibid.* **34**, 2439 (1986).

[25] R. M. Nieminen, in *Positron Solid State Physics*, edited by W. Brandt and A. Dupasquier (North-Holland, Amsterdam, 1983); E. Boroński and R. M. Nieminen, Phys. Rev. B **34**, 3820 (1986).

[26] M. J. Puska, J. Phys.: Condens. Matter **3**, 3455 (1991); F. Plazaola, A. P. Seitsonen, and M. J. Puska, *ibid.* **6**, 8809 (1994).

[27] S. Kahana, Phys. Rev. **129**, 1622 (1963); W. Brandt and J. Reinheimer, Phys. Lett. A **35**, 109 (1971); J. Arponen and E. Pajanne, J. Phys. C **12**, 3013 (1979). Function $\gamma^h(n_0)$ was parametrized by Barbiellini *et al.* (Ref. 13), and $V_{corr}(n_0)$ was parametrized by Boroński and Nieminen (Ref. 25); J. Arponen and E. Pajanne, J. Phys. F: Met. Phys. **9**, 2359 (1979), provided momentum-dependent correlation functions $\epsilon[(E/E_F),n_0]$; [also see A. Kallio, P. Pietiläinen, and L. Lantto, Phys. Scr. **25**, 943 (1982)]. Function $\gamma^h(n_0)$ was parametrized by E. Boroński and R. M. Nieminen (Ref. 25). Function $\gamma^h(n_0)$ and enhancement factors $\epsilon[(E/E_F),n_0]$ were parametrized by H. Stachowiak and J. Lach, Phys. Rev. B **48**, 9828 (1993); [also see H. Stachowiak, Phys. Rev. B **41**, 12 522 (1990)].

[28] A. Rubaszek and H. Stachowiak [Phys. Status Solidi B **124**, 159 (1984); Phys. Rev. B **38**, 3846 (1988)]; and A. Rubaszek, H. Stachowiak, E. Boroński, and Z. Szotek [*ibid.* **30**, 2490 (1984)], provide momentum-dependent correlation functions $\epsilon[(E/E_F),n_0]$.

[29] A. K. Singh and T. Jarlborg, J. Phys. F: Met. Phys. **15**, 727 (1985); T. Jarlborg and A. K. Singh, Phys. Rev. B **36**, 4660 (1987).

[30] P. Harthoorn and P. E. Mijnarends, J. Phys. F: Met. Phys. **8**, 1147 (1978).

[31] D. G. Lock, V. H. C. Crisp, and R. N. West, J. Phys. F: Met. Phys. **3**, 561 (1973).